iScience

CellPress
OPEN ACCESS

Article

Selective postnatal excitation of neocortical pyramidal neurons results in distinctive behavioral and circuit deficits in adulthood

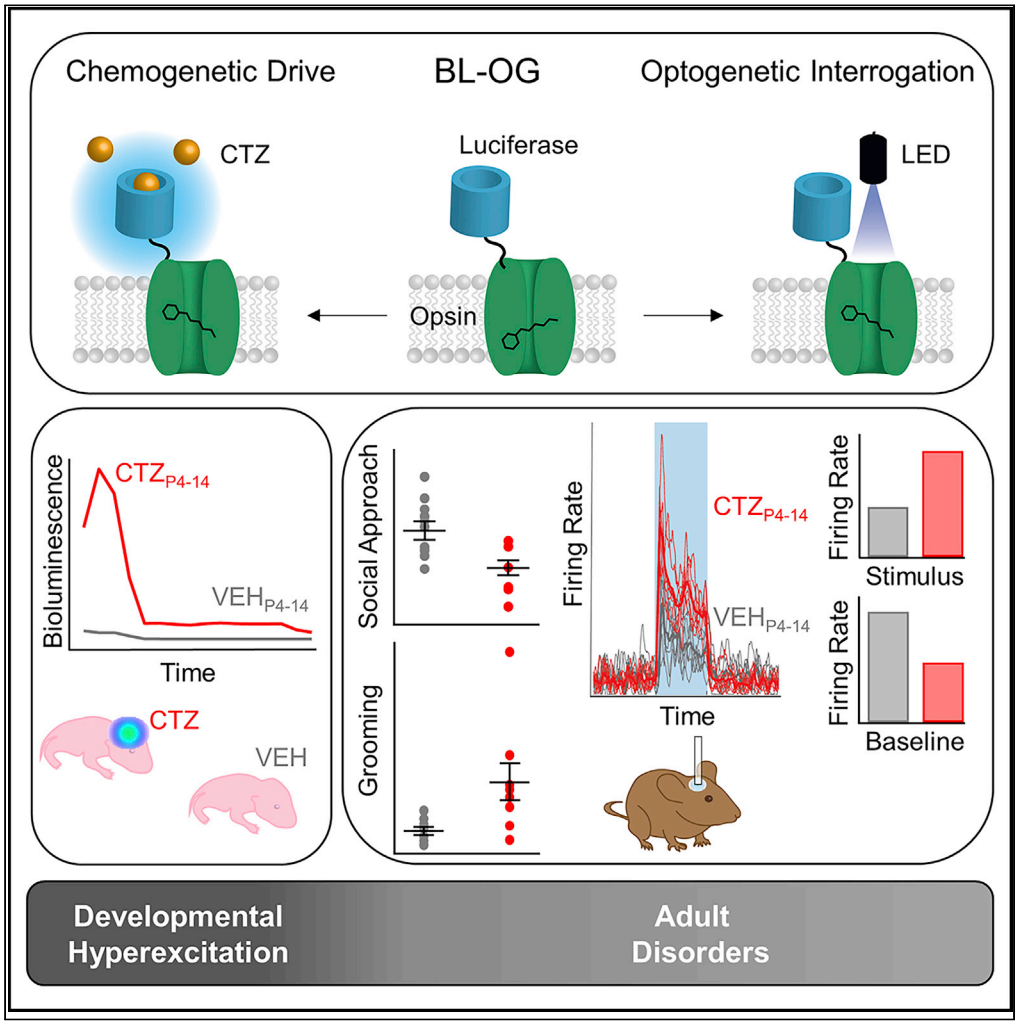

William E. Medendorp, Andreas Bjorefeldt, Emmanuel L. Crespo, ..., Madison L. Waddell, Christopher I. Moore, Ute Hochgeschwender

christopher_moore@brown.edu (C.I.M.)
hochg1u@cmich.edu (U.H.)

HIGHLIGHTS

BL-OG allows chemogenetic activation and optogenetic interrogation in the same animal

Developmental hyperexcitation in normal mice leads to neurodevelopmental disorders

In these mice adult neurons show reduced baseline activity and increased excitability

Reduced activity-triggered coherence and altered oscillations in cortex and striatum

Medendorp et al., iScience 24, 102157
March 19, 2021
https://doi.org/10.1016/j.isci.2021.102157

iScience

CellPress
OPEN ACCESS

Article

Selective postnatal excitation of neocortical pyramidal neurons results in distinctive behavioral and circuit deficits in adulthood

William E. Medendorp,[1,2] Andreas Bjorefeldt,[1,3] Emmanuel L. Crespo,[1,2] Mansi Prakash,[2] Akash Pal,[1,2] Madison L. Waddell,[1] Christopher I. Moore,[3,4,*] and Ute Hochgeschwender[1,2,5,*]

SUMMARY

In genetic and pharmacological models of neurodevelopmental disorders, and human data, neural activity is altered within the developing neocortical network. This commonality begs the question of whether early enhancement in excitation might be a common driver, across etiologies, of characteristic behaviors. We tested this concept by chemogenetically driving cortical pyramidal neurons during postnatal days 4–14. Hyperexcitation of Emx1-, but not dopamine transporter-, parvalbumin-, or Dlx5/6-expressing neurons, led to decreased social interaction and increased grooming activity in adult animals. *In vivo* optogenetic interrogation in adults revealed decreased baseline but increased stimulus-evoked firing rates of pyramidal neurons and impaired recruitment of inhibitory neurons. Slice recordings in adults from prefrontal cortex layer 5 pyramidal neurons revealed decreased intrinsic excitability and increased synaptic E/I ratio. Together these results support the prediction that enhanced pyramidal firing during development, in otherwise normal cortex, can selectively drive altered adult circuit function and maladaptive changes in behavior.

INTRODUCTION

Internally generated neural activity during brain development is critically involved in the configuration of connections. In this context, experience-dependent activity builds further synapse formation, elimination, and rearrangements during development and throughout life (Andreae and Burrone, 2014; Golshani et al., 2009; Katz and Shatz, 1996; Penn and Shatz, 1999). Presumably, alterations in intrinsic excitability, and concomitant changes in internally and externally dependent driven activity, underlie neurological and psychiatric disorders. Consistent with this view, a wealth of studies in adult animals have implicated altered neocortical excitatory-inhibitory (E/I) balance in the etiology of autism spectrum disorder (ASD) and other neurodevelopmental disorders, with a net shift toward excitation (Nelson and Valakh, 2015; Rubenstein and Merzenich, 2003; Sohal and Rubenstein, 2019). Recent work analyzing multiple mouse models of ASD has found that net decrease in inhibitory transmission can be relative, as excitatory and inhibitory synapses are both weakened (Antoine et al., 2019). Although acute changes in adult E/I balance can induce and reduce ASD phenotypes (Selimbeyoglu et al., 2017; Yizhar et al., 2011), whether these changes can result from early life alterations to the excitability of pyramidal neurons, or whether this shift has different mechanistic origins, is not known.

To directly address whether early life alterations in pyramidal activity can induce adult phenotypes and related circuit changes, we systematically enhanced pan-neocortical pyramidal activity levels in early development in healthy mice using non-invasive BioLuminescent-OptoGenetic (BL-OG)-mediated chemogenetics (Berglund et al., 2013, 2016; Moore and Berglund, 2020). By activating Emx1-positive neurons, we found that developmental pyramidal over-drive in otherwise healthy subjects selectively led to decreased social interaction and increased grooming activity in adult animals, two key symptoms of ASD. *In vivo*, both prefrontal neural activity and functional markers of cortico-striatal connectivity were impaired in over-excited Emx1-positive mice, and *ex vivo* slice recordings revealed alterations to both intrinsic excitability and synaptic E/I ratio in L5 prefrontal cortex pyramidal neurons. These data show that brief and selective increases in pyramidal activity over a limited developmental window can generate key behavioral and neurophysiological signatures of ASD. As such, they implicate aberrant neocortical pyramidal activity during early development as a potential common driver of ASD-like phenotypes.

[1]Program in Neuroscience, Central Michigan University, Mount Pleasant, MI 48859, USA

[2]College of Medicine, Central Michigan University, Mount Pleasant, MI 48859, USA

[3]Department of Neuroscience, Brown University, Providence, RI 02906, USA

[4]Carney Institute for Brain Science, Brown University, Providence, RI 02906, USA

[5]Lead contact

*Correspondence: christopher_moore@brown.edu (C.I.M.), hochg1u@cmich.edu (U.H.)

https://doi.org/10.1016/j.isci.2021.102157

RESULTS

Developmental hyperexcitation of Emx1 pyramidal neurons is distinctive in causing behavioral phenotypes

To stimulate genetically targeted neural circuits, we employed bioluminescent optogenetics (BL-OG) (Berglund et al., 2013, 2016; Gomez-Ramirez et al., 2020; Park et al., 2020; Song et al., 2018; Yu et al., 2019; Zenchak et al., 2020). This approach has the distinct dual advantage of enabling both non-invasive chemogenetic manipulation and temporally selective optogenetic control with the same molecular construct. In the BL-OG approach, an optogenetic element can be activated either by light emitted from a tethered luciferase oxidizing a small molecule substrate or by light emitted from physical sources, such as LEDs or lasers (Figure 1A). To activate brain-wide genetically defined populations in a distinct period in early development, we generated a conditional mouse line expressing the excitatory luminopsin 3 (LMO3) in a Cre-dependent manner (Figure S1). Crossing the lox-stop-lox (LSL)-LMO3 line to Cre driver mouse lines enabled hyperexcitation of defined neural populations (Figure 1B).

We induced hyperexcitation in developing mouse pups once a day during post-natal days 4–14, capturing the window of significant outgrowth and development of key cortical circuits (Romand et al., 2011; Sasaki et al., 2015). BL-OG has been used to both activate and silence neurons in adult mice and rats, using various routes of administration of CTZ (Berglund et al., 2016; Gomez-Ramirez et al., 2020; Park et al., 2020; Tung et al., 2015; Yu et al., 2019). To confirm the efficacy of BL-OG in pups, we tested for bioluminescence emission and neural activity after intraperitoneal CTZ administration. Bioluminescence emission occurred within 10–15 min and declined over the following hour in Emx1-LMO3 expressing, but not in non-expressing, pups (Figure 1B inset). Neural activity followed a similar timeline when we recorded spikes from putative layer 5 medial prefrontal cortex (mPFC) pyramidal neurons *in vivo* in P12–P14 pups (Figure S2A). The results in pups regarding onset of activity changes due to CTZ and duration of the effect resemble those obtained in adult animals (Berglund et al., 2016), including the correspondence of bioluminescence increases with higher firing rates (Gomez-Ramirez et al., 2020). We also recorded in slices from P7 Emx1-LMO3 pups, where brief bath application of CTZ depolarized the membrane potential and increased the firing response to current stimulation (Figure S2B). Taken together, our results demonstrate the suitability of using a conditional BL-OG system for exploring the effects of developmental hyperexcitation.

In developing pups, the effect of selective hyperexcitation was examined in multiple neural populations (Figure 1C). We employed the Emx1-Cre line to enhance pan-neocortical pyramidal activity (Gorski et al., 2002), Pvalb-Cre to target inhibitory neurons of the cortex (Hippenmeyer et al., 2005), and Dlx5/6-Cre to target GABAergic neurons of the forebrain (Monory et al., 2006). In complement to targeting these cell types focally creating E/I balance in cortex, we also targeted the dopaminergic system using the DAT-Cre mouse (Backman et al., 2006).

Stimulation of selected neural populations was limited to the postnatal period P4–14, after which the animals received no further CTZ application. To test the prediction that behavioral phenotypes will emerge from over-excitation of distinct neural populations during development, we assayed selected behaviors associated with neurodevelopmental disorders (Silverman et al., 2010), including social interaction, stereotypic behavior, and anxiety (Figure 1D). Selective developmental BL-OG activation of pyramidal neurons, but not interneurons or dopaminergic systems, generated key ASD phenotypes of reduced social behavior and increased compulsivity, as well as hypo-locomotion. Developmentally hyperexcited Emx1-LMO3 mice showed significantly reduced interaction times during the social approach test in a three-chamber setting (Figures 1D and S3). Social interaction was measured as time spent by the test animal actually interacting within a 1-inch radius with the stationary mouse, with Emx1-LMO3 showing significantly reduced time spent interacting (students t test: $t(18) = 3.07$, $p = 0.0067$). To disambiguate changes in social preference from those in overall exploration or activity, we conducted a two-way ANOVA test with dependent variable of time spent in a chamber and independent variables of chamber type (empty or with stationary mouse) and genotype (control or experimental). We found a significant interaction of chamber by genotype ($F(2,54) = 7.26$, $p = 0.0016$). Further post-hoc analysis revealed Emx1-LMO3 mice spent significantly less time in the chamber with the stationary mouse compared with controls (Tukey's post-hoc: $p < 0.05$). No significant main effect was found for chamber, indicating no bias was found for any one chamber across groups. In the social novelty test, Emx1-LMO3 mice showed no significant differences from controls on time spent interacting with the novel mouse (students t test: $t(18) = 1.97$, $p = 0.0650$). Pvalb-LMO3 mice demonstrate over 50% reduced time spent interacting with the novel mouse compared with non-expressing

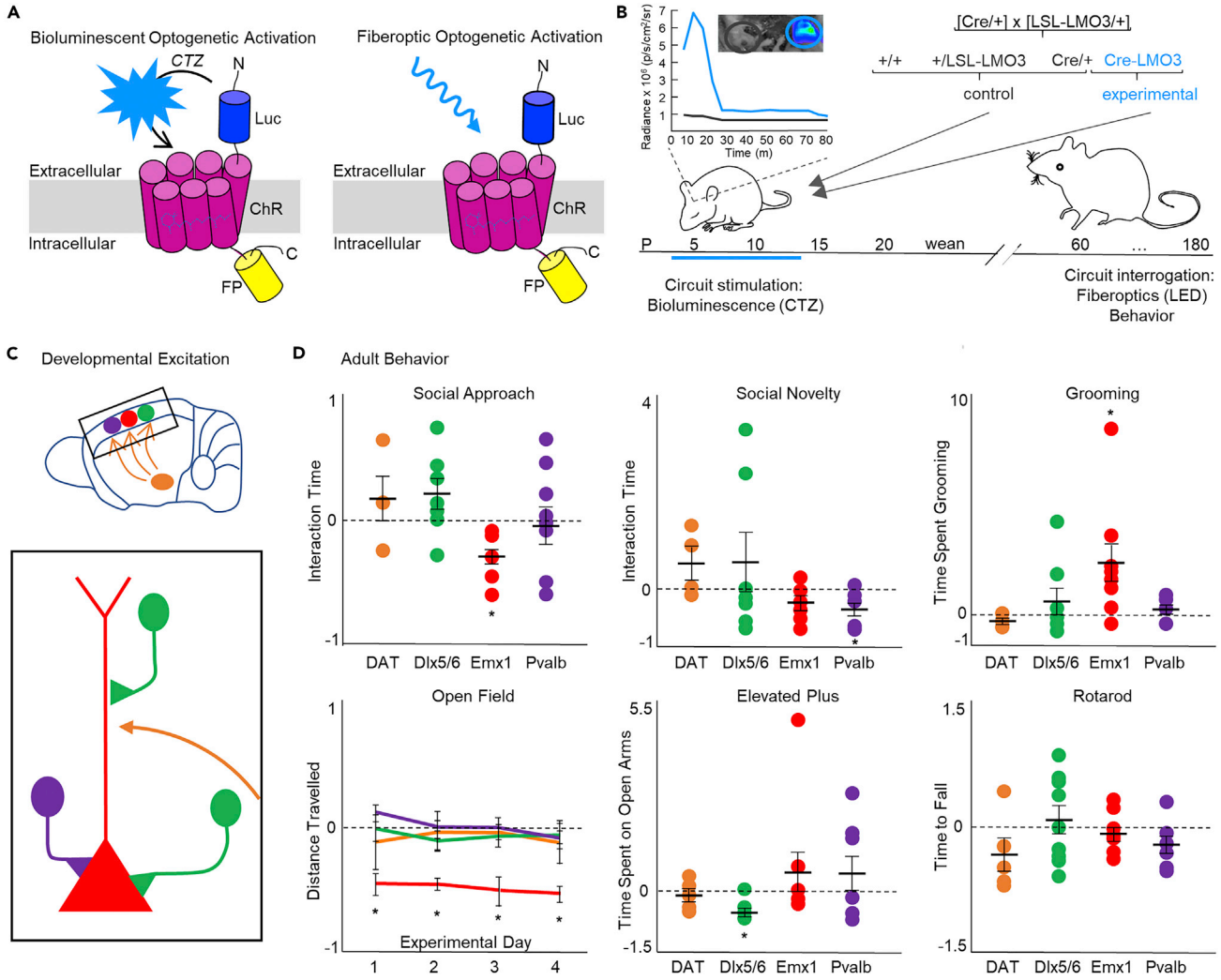

Figure 1. Developmental hyperexcitation of Emx1 pyramidal neurons is distinctive in causing behavioral phenotypes

(A) Schematics of a luminopsin (Luc, luciferase, is tethered to ChR, channelrhodopsin; FP, fluorescent protein). Application of the small molecule substrate coelenterazine (CTZ) results in production of photons and bioluminescent optogenetic activation of the nearby opsin (left). The same molecule is accessible to stimulation by a physical light source for standard fiberoptic optogenetic activation (right).

(B) Experimental design. Heterozygous Cre driver mice (Cre/+) were mated with heterozygous conditional (lox-stop-lox) luminopsin-3 mice (LSL-LMO3/+), generating three groups of control mice and one group of experimental mice expressing LMO3 in cells specified by the Cre driver (Cre-LMO3). All pups of a litter were injected once a day intraperitoneally with CTZ postnatal days 4–14. Inset shows representative example of IVIS imaging of Emx1-LMO3 positive and negative pup and ROIs plotted over time. See also Figures S1 and S2.

(C) Schematics of circuits targeted for developmental hyperexcitation. Color codes are used consistently for C and D: red—Emx1, green—Dlx5/6, purple—Pvalb, orange—DAT.

(D) Adult behavior of developmentally hyperexcited mice. Each group of Cre (DAT, Dlx5/6, Emx1, Pvalb)-LMO3 mice is normalized to their non-LMO3 expressing controls. Bars represent mean ± SEM.

See also Figure S3. N = 5-9 per group. *p < .05, see also Table S1.

littermates (students t test: t(21) = 2.19, p = 0.0398) but showed no differences from controls in social approach. DAT-LMO3 and Dlx6a-LMO3 mice did not show significant differences versus littermate controls during either the social approach test or the social novelty test (see also Figure S3 and Table S1). Emx1-LMO3 mice were the only group to exhibit evidence of repetitive behaviors, showing significantly increased time spent grooming by 250% compared with non-expressing littermates (student's t test: t(18) = −2.92, p = 0.0091; Figures 1D and S3). Emx1-LMO3 mice again were the only cohort to demonstrate altered exploration in open field, displaying significantly reduced movements over time (two-way repeated measures ANOVA—main effect between groups: F(1,14) = 11.56, p = 0.0043; Figures 1D and S3). These behavioral

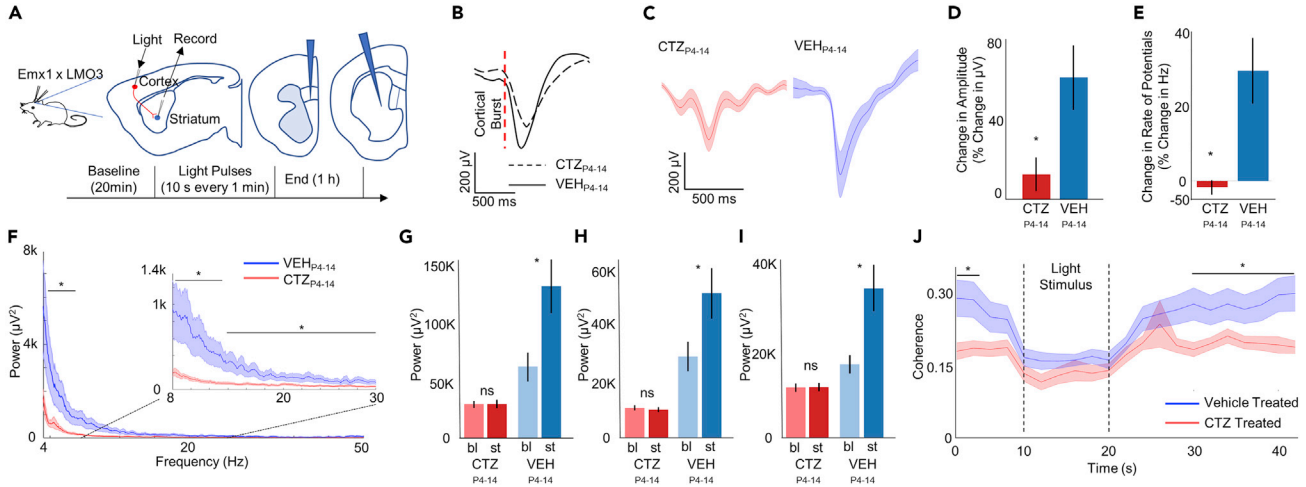

Figure 2. Developmental pyramidal hyperexcitation leads to decreased cortico-striatal communication

(A) Schematic of experimental setup. Laminar probes were inserted in the prelimbic area of the medial prefrontal cortex and the striatum.

(B) Striatal event-related local field potentials (erLFPs) time locked to cortical action potential bursts (2 spikes in 10 ms) for adult Emx1-LMO3 mice developmentally stimulated (CTZP4-14, N = 5) and controls (VEHP4-14, N = 5).

(C) erLFPs during optogenetic stimulation: CTZP4-14 mice (red) demonstrate smaller negative deflections compared with VEHP4-14 mice (blue). Shaded area represents mean ± SEM.

(D) Amplitude changes of erLFPs during optogenetic stimulus normalized to baseline before stimulus. Bars represent mean ± SEM.

(E) Frequency changes among erLFPs during optogenetic stimulus normalized to baseline before stimulus. Bars represent mean ± SEM.

(F) Power spectra of striatal neurons during light stimulus for CTZP4-14 (red)- and VEHP4-14 (blue)-treated groups. Shaded area represents mean ± SEM.

(G–I) Average power spectra for the Theta (G), Alpha (H), or Beta (I) range during baseline (bl) and stimulus (st) conditions for both CTZP4-14- and VEHP4-14-treated groups. Bars represent mean ± SEM.

(J) Coherence between cortex and striatum for both CTZP4-14 (red)- and VEHP4-14 (blue)-treated mice before, during and after optogenetic stimulus. Shaded area represents mean ± SEM. *p < .05, see also Table S1.

effects were selective to pyramidal activation: interneuron drive, for example in the Dlx5/6 group, had opposing effects. Further, the pyramidal activation had selective behavioral effects: developmental hyperexcitation of Emx1 neurons did not result in changes in anxiety for which imbalances in excitatory glutamatergic and inhibitory GABAergic circuits have been implicated (Depino et al., 2008). Indeed, developmental hyperexcitation of GABAergic Dlx5/6 neurons caused mice to display evidence of increased anxiety. These mice spent significantly reduced time on the open arms during the elevated plus maze compared with non-expressing littermates (log-transformed data, student's t test: $t(23) = 2.52$, $p = 0.0096$; Figures 1D and S3). To test whether these interventions affected basic coordination, we employed the rotarod, a commonly used metric of basic learning and coordination. No significant differences on time to fall were observed in any of the developmentally treated mice compared with non-expressing littermates (Figures 1D and S3).

Developmental pyramidal hyperexcitation leads to decreased cortico-striatal communication

Studies in humans and mouse models directly indicate that cortico-striatal communication is altered in neurodevelopmental disorders with basal ganglia association, such as Tourette and obsessive-compulsive disorders. Also, many ASD models show altered connectivity between the cortex and the striatum (Martella et al., 2018; Nagarajan et al., 2018; Peca et al., 2011; Rothwell et al., 2014; Shofty et al., 2019; Wang et al., 2016). To probe cortico-striatal communication in the relay of endogenous and controlled neocortical events, we measured the impact of naturally occurring neocortical bursts and induced optogenetic bursts on striatal evoked potential responses. Recordings were carried out in adult Emx1-LMO3 mice treated during postnatal days 4–14 with CTZ (CTZ_{P4-14} mice) or with vehicle (VEH_{P4-14} mice). Use of LMOs enables optogenetic access to the same Emx1 pyramidal neurons initially hyperexcited chemogenetically during development. We placed laminar electrodes in the medial prefrontal cortex (layer 5) and the dorsal striatum (Figure 2A). After 20 min of baseline, mice received acute stimulation to the prefrontal cortex through light pulses of 10s separated by 1-min intervals. To identify changes in striatal responses between baseline and light stimulus periods, event-related local field potentials (erLFP) were captured after optogenetic-stimulus-induced bursts of cortical activity (Figures 2B–2E, 5 mice per group, 35 trials). Spike-triggered LFPs provide a measure of cortical input, allowing indirect measure of change in effective

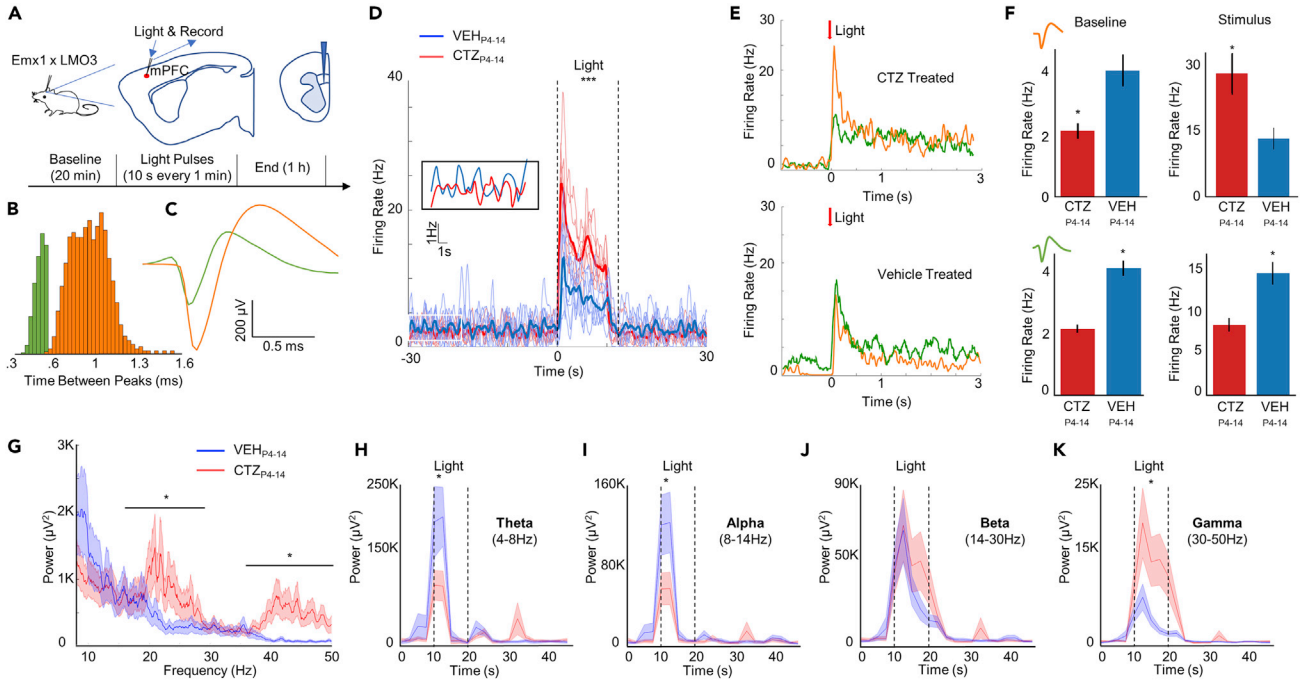

Figure 3. Developmental pyramidal hyperexcitation leads to decreased baseline firing, enhanced stimulus-evoked firing, and decreased output connectivity in pyramidal neurons

(A) Schematic of experimental setup. Laminar probes were inserted in the prelimbic area of the medial prefrontal cortex.

(B) Waveforms were sorted based on time between peaks. Histogram of these peak to peak times shows a cluster of inhibitory neurons (green) and pyramidal neurons (orange).

(C) Traces of waveforms from putative inhibitory (green) and pyramidal neurons (orange).

(D) The group effects of optogenetic stimulation: CTZP4-14-treated mice show lower baseline levels (inset) and a consistently larger response to stimulation compared with VEHP4-14-treated mice, N = 5 per group.

(E) Light-dependent responses by pyramidal and interneuron populations: CTZP4-14 mice (upper panel) show far greater pyramidal neuron response (orange trace) to light stimulation, whereas VEHP4-14 mice (lower panel) show greater interneuron response (green trace) to light stimulation.

(F) Average firing rate for each group by neuron type and by time point (baseline or stimulus). Bars show mean ± SEM (upper panel—pyramidal neurons, lower panel—inhibitory neurons).

(G) Time-independent power-spectra of cortical neuron LFP during light stimulus. Shaded area represents mean ± SEM.

(H–K) Power over time before, during and after light stimulus for Theta (H), Alpha (I), Beta (J), and Gamma (K) frequency ranges. Shaded area represents mean ± SEM. *p < .05, see also Table S1.

communication (Syed et al., 2011). CTZ_{P4-14} mice showed significantly reduced amplitude during baseline conditions (ANOVA: $F(3,11752) = 51.28$, $p < 0.0001$; Bonferroni post-hoc: $p < .001$; Figures 2B and 2C), suggesting weaker descending excitatory drive. Similarly, CTZ_{P4-14} mice showed no significant differences in the amplitude of erLFPs evoked by light stimulus versus the baseline (Bonferroni post-hoc: $p = 0.913$; Figure 2D). VEH_{P4-14} mice, by contrast, showed significantly larger amplitude responses to light stimulation (Bonferroni post-hoc: $p < 0.001$; Figure 2D). Frequency of LFPs during baseline was not significantly different between groups; however, CTZ_{P4-14} mice showed a generalized decline in frequency power during the light stimulus, whereas the VEH_{P4-14} group displayed an increase (Mann-Whitney: $z -1.964$, $p = 0.0496$; Figure 2E). Ongoing population activity was also different between the groups during optical stimulation, as CTZ_{P4-14} mice showed significantly lower power in the striatum (Theta: $F(3,108) = 3.19$, $p = 0.0265$; Alpha: $F(3,108) = 3.48$, $p = 0.0184$; Beta: $F(3,108) = 3.40$, $p = 0.0204$; Figure 2F). This decrease in the Beta and Gamma bands in striatum is notable, given the robust increase in their expression during optogenetic drive of cortical pyramidal neurons (see Figure 3), supporting the suggestion of a functional decrease in connection between these key forebrain structures. Baseline- and optical-stimulation-associated power spectra revealed no significant change among CTZ_{P4-14} mice during light stimulus in either the Theta, Alpha, or Beta frequency ranges, indicating no increased response to incoming neocortical signals (Bonferroni post-hoc: $p = 1.0$; Figures 2G–2I). VEH_{P4-14} mice, by contrast, showed significantly elevated power during light stimulus compared with baseline in all three frequency ranges (Bonferroni post-hoc, Theta: $p = 0.050$; Alpha: $p = 0.036$; Beta: $p = 0.042$). Based on these several indicators of decreased input

connectivity, we also directly measured signal coherence (Kramer, 2013). CTZ_{P4-14} mice exhibited significantly lower coherence before and after light stimulus (Interaction of Time x Group: $F(20,1128) = 1.87$, $p = 0.0117$; Figure 2J), consistent with a broad decrease in coupling efficiency between the two structures. Coherence in both groups declined during the light stimulus to near chance levels. Although based on indirect measurements, our findings fit well into results from prior studies that have shown that cortico-striatal communication in ASD models transitions across development, with early enhancement and adult degradation (Peixoto et al., 2016, 2019; Peca et al., 2011; Wang et al., 2016).

Developmental pyramidal hyperexcitation leads to decreased baseline firing, enhanced stimulus-evoked firing, and decreased output connectivity in pyramidal neurons

Alterations in ASD-associated proteins can create profound decreases in homeostatic plasticity, directly implicating such dynamics in evolution of the disorder (Tatavarty et al., 2020). Such changes may manifest through changes in intrinsic excitability and/or synaptic communication. To directly test the impact of developmental hyperexcitation of pyramidal neurons, we measured neural activity in mPFC of adult Emx1-LMO3 animals developmentally treated with CTZ (CTZ_{P4-14} mice) or with vehicle (VEH_{P4-14} mice).

Recordings of cortical activity were conducted using a laminar probe traversing all layers of the cortex (Figure 3A). Spikes sorting identified putative fast-spiking interneuron and pyramidal neuron subtypes (Figures 3B and 3C). In agreement with the basic prediction of a tonic decrease in network-level excitability, we found a lower baseline firing rate among putative pyramidal neurons in CTZ_{P4-14} mice (Figure 3D inset). Interestingly, these same cells consistently showed a larger increase in firing rate in response to direct optogenetic drive compared with VEH_{P4-14} mice (two-way repeated measures ANOVA, main effect between groups: $F(1,6) = 6.86$, $p = 0.0396$; Figure 3D). No effect was found by trial number, indicating the light stimulus did not produce differential effects depending on when the trial occurred (main effect for trial: $F(6,36) = 1.38$, $p = 0.2494$). No significant differences were found in the maximum firing rate between groups (main effect between groups: $F(1,6) = 1.30$, $p = 0.2977$), demonstrating that VEH_{P4-14} mice do reach a similar firing rate later in the light stimulation. Average firing rates after acute light stimulus between pyramidal neurons and interneurons revealed lower rates for interneurons relative to the increased rates for pyramidal neurons in CTZ_{P4-14} mice, whereas interneurons showed a slightly higher response than pyramidal neurons in VEH_{P4-14} mice (Figure 3E). During baseline, CTZ_{P4-14} mice showed significantly reduced activity among pyramidal neurons in the cortex compared with VEH_{P4-14} mice (Students t test: $t(7) = -6.082$, $p = 0.0005$; Figure 3F, upper panel). During light stimulus, by contrast, CTZ_{P4-14} mice displayed significantly *increased* pyramidal firing rates compared with VEH_{P4-14} mice ($t(7) = 2.541$, $p = 0.0386$). For interneurons, firing rates were significantly reduced in CTZ_{P4-14} mice at baseline (Students t test: $t(7) = 2.526$, $p = 0.0395$) and, different from pyramidal neurons, were also recruited less effectively by light stimulation (Students t test: $t(7) = -2.41$, $p = 0.0468$; Figure 3F, lower panel).

These optogenetic results suggest that pyramidal recruitment of feedback inhibition by fast-spiking interneurons is diminished in CTZ_{P4-14} mice. Several studies have demonstrated that altered E/I dynamics at many different points in the neocortical networks can result in altered neural oscillations (Atallah and Scanziani, 2009; Brunel and Wang, 2003; Carlén et al., 2012). These studies suggest that an altered ratio toward excitation can result in a shift in neural oscillations to higher power in the lower Gamma range (30–80 Hz). To assess whether oscillatory dynamics are altered in CTZ_{P4-14} mice, we analyzed power spectra of the LFP signal (Figure 3G). During light stimulus, CTZ_{P4-14} mice showed significantly greater power in the Beta and the Gamma range (Student's t test: $t(6) = 2.517$, $p = 0.0455$; $t(6) = 2.732$, $p = 0.0341$), suggesting these mice may experience altered excitation/inhibition balance. Given the elevated power in the Beta and Gamma range among CTZ_{P4-14} mice, we assessed how these oscillations change over time. Fast Fourier transforms performed before, during, and after light stimulation revealed a burst-like increase in the Theta and Alpha frequency ranges (two-way repeated measures—interaction of time x group: Theta: $F(20,1128) = 3.21$, $p < 0.0001$; Alpha: $F(20,1128) = 3.49$, $p < 0.0001$; Figures 3H and 3I). The differences occur within the first few seconds of light stimulation (Bonferroni post-hoc: Theta: $p = 0.0203$; Alpha: $p = 0.0302$), with the power returning to baseline levels roughly half-way through the light stimulus. In the Beta and Gamma range, power increases were sustained for the length of light stimulation (Figures 3J and 3K). VEH_{P4-14} mice and CTZ_{P4-14} mice exhibit different responses to light stimulation. In lower frequencies, the burst-like response was damped in CTZ_{P4-14} mice (two-way repeated measures—interaction of time x group: Theta: $F(20,1128) = 3.21$, $p < 0.0001$; Alpha: $F(20,1128) = 3.49$, $p < 0.0001$; Figures 3H and 3I). Although a main effect of differences in the Beta power was observed (Figure 3G), putatively due to an evolving

difference with sustained stimulation (Figure 3J), no significant differences were found between individual time points ($F(20,1128) = 0.78$, $p = 0.7392$). In the Gamma frequency range, CTZ_{P4-14} mice showed significantly higher power compared with VEH_{P4-14} mice (two-way repeated measures—interaction of time x group: $F(20,1128) = 5.40$, $p < 0.0001$; Figure 3K).

Developmental pyramidal hyperexcitation produces enduring alterations in intrinsic excitability and synaptic E/I ratio of L5 prefrontal cortex pyramidal neurons

To elaborate on cellular and synaptic mechanisms to explain the observed effects of developmental hyperexcitation on neural activity in prefrontal cortex *in vivo*, we recorded from Emx1-LMO3 positive layer 5 (L5) pyramidal neurons in prefrontal cortex slices from young adult (P30–40) animals that received either CTZ_{P4-14} or VEH_{P4-14} (Figure 4A).

We first examined the intrinsic firing properties of L5 pyramidal neurons in the presence of synaptic blockers (D-AP5, CNQX, picrotoxin) and found the firing threshold was significantly increased in CTZ_{P4-14} animals (-30 ± 1.4 mV versus -44.2 ± 1.8 mV, Figures 4B and 4E). In response to depolarizing square current injections of increasing magnitude (Figures 4C and 4D), CTZ_{P4-14} L5 pyramidal neurons displayed an increased rheobase current (242.9 ± 16.5 pA versus 146.2 ± 22.6 pA, Figure 4E) as well as a lower maximum firing frequency ($21 \pm$

2.7 Hz versus 42 ± 2.9 Hz, Figure 4E), resulting in a pronounced right-shift of the frequency-current (f-I) curve. No significant effect on input resistance was observed between groups (82.6 ± 6.6 MΩ versus 86.9 ± 6.6 MΩ, Figure 4E). These results suggest that sustained developmental hyperexcitation of Emx1 positive pyramidal neurons leads to an intrinsically hypoexcitable phenotype in adulthood.

To evaluate the net effect of developmental hyperexcitation on synaptic efficacy onto pyramidal neurons in the prefrontal network, we performed voltage-clamp recordings of miniature excitatory and inhibitory postsynaptic currents (mEPSCs/mIPSCs) from LMO3 positive L5 cells at −70 and +10 mV, respectively, in the presence of tetrodotoxin. We found no significant change in the frequency (13 ± 1.5 Hz versus 10.6 ± 1.3 Hz, Figures 4F and 4G) or amplitude (17.2 ± 0.9 pA versus 16.1 ± 1.1 pA, Figures 4F and 4G) of mEPSCs between groups. In contrast, we found that both the frequency (28.6 ± 2.7 Hz versus 42 ± 5.1 Hz, Figures 4H and 4I) and amplitude (24.5 ± 1.5 pA versus 32.5 ± 3.6 pA, Figures 4H and 4I) of mIPSCs were significantly reduced in CTZ_{P4-14} animals, indicating a net decrease in synaptic efficacy of $GABA_A$-ergic transmission. The respective effects on frequency and amplitude of mEPSCs and mIPSCs between groups resulted in increased E/I ratios in CTZ_{P4-14} mice (frequency: 0.49 ± 0.06 versus 0.3 ± 0.05; amplitude: 0.73 ± 0.04 versus 0.53 ± 0.04; Figure 4J), producing a 2-fold increase in E/I ratio of synaptic drive (0.36 ± 0.05 versus 0.17 ± 0.04, Figure 4J). Together these results show chronic excitation of Emx1 neurons during early development produces lasting changes to intrinsic excitability and functional connectivity of L5 pyramidal neurons of the prefrontal cortex, where a reduction in intrinsic excitability is accompanied by a lowered synaptic efficacy of inhibitory transmission.

DISCUSSION

Here, we tested in healthy animals the impact of early enhancement in neural activity within specific cell types. We found that early hyperexcitation of pyramidal neurons alone, and for a limited time window, is sufficient to create adult neurophysiological and behavioral phenotypes in the absence of other genetic or environmental insults. Moreover, early postnatal interference with neural activity of other distinct populations resulted in different behavioral symptoms, indicating selective effects. In addition to causally linking developmental neural activity with adult behavior, our results provide insights into the dynamics of neural networks responding to aberrant activity patterns during development.

The sufficiency of brief hyperexcitability to derail circuit formation in an otherwise normal brain highlights an underappreciated vulnerability of developing neural circuits where seemingly innocuous events can have lifelong behavioral consequences. This finding may provide an explanation for the large variety of potential etiologies reported for symptoms of ASD and other neurodevelopmental disorders, with infections, autoimmune processes, and environmental causes acting in concert with genetic and epigenetic susceptibilities (Amaral, 2017; Grandjean and Landrigan, 2006; Jones and Van de Water, 2019; Landrigan, 2010; Mawson and Croft, 2019; Roberts et al., 2019; Tartaglione et al., 2019).

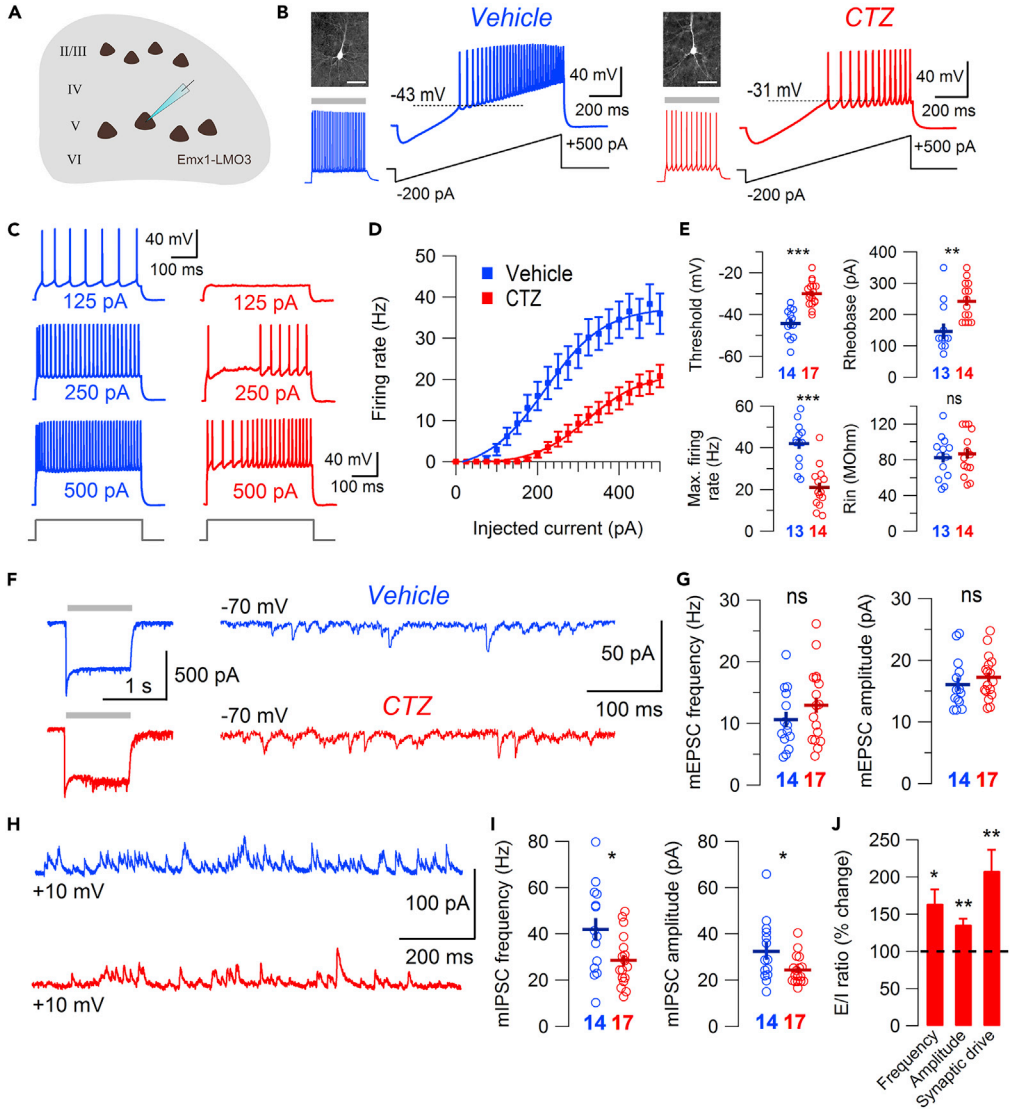

Figure 4. Developmental pyramidal hyperexcitation produces enduring alterations in intrinsic excitability and synaptic E/I ratio of L5 prefrontal cortex pyramidal neurons

(A) Schematic of mouse prefrontal cortex brain slice featuring LMO3 pyramidal neurons.

(B) Firing response of biocytin-filled L5 prefrontal cortex pyramidal neurons to depolarizing current ramps (dotted line indicates threshold) in VEHP4-14 (blue) and CTZP4-14 (red) groups (scale bars: 100 μm). LMO3 expression confirmed with blue light stimulation.

(C) Example traces of firing response to depolarizing square current injections of increasing magnitude.

(D) Frequency-current relationship of L5 pyramidal neurons. Bars represent mean ± SEM.

(E) Summary graphs showing effect of developmental hyperexcitation on firing threshold, rheobase, maximum firing rate, and input resistance. Bars represent mean ± SEM.

(F) Example traces of mEPSCs recorded from LMO3 positive L5 pyramidal neurons (LMO3 expression confirmed with blue light stimulus at −70 mV, left).

(G) Summary graphs showing effect of developmental hyperexcitation on mEPSC frequency and amplitude. Bars represent mean ± SEM.

(H) Example traces of mIPSCs recorded from LMO3 positive L5 pyramidal neurons.

(I) Summary graphs showing effect of developmental hyperexcitation on mIPSC frequency and amplitude. Bars represent mean ± SEM.

(J) Summary graph showing effect of developmental hyperexcitation on E/I ratio of mPSC frequency, amplitude, and synaptic drive. Bars represent mean ± SEM. *p < 0.05, **pP < 0.01, ***p < 0.001. See also Table S1.

An increased E/I ratio in the cortical network, resulting from overexcitation of pyramidal neurons, impaired GABAergic inhibition, or both, has remained central in ASD research (Rubenstein and Merzenich, 2003; Sohal and Rubenstein, 2019). Our data both *in vivo* and *ex vivo* show that inappropriate "E/I balance" may be most important to disease development if expressed, even for just a narrow window, early in development, and that imbalance during this window is sufficient in driving a cascade leading to phenotypic behavioral and circuit outcomes in the disorder.

The use of the BL-OG control strategy here uniquely enabled this study. Combined chemogenetic and optogenetic access through the same genetically targeted molecule provided developmental perturbation and adult functional probe of system connectivity and excitability. This approach offers an experimental framework for delineating developmental network disturbances and their consequences in establishing adult neural connections and their resulting behaviors in the general field of neurodevelopmental disorders.

Limitations of the study

In this study, we tested the effects of hyperexcitation over a relatively broad temporal window, P4–14, that covers a range of postnatal developmental events. This time window is sufficient to create the observed behavioral and electrophysiological changes in adults. However, this result does not mean that this particular developmental window will be the only one to create the effects observed. In fact, it will be interesting in future studies both to break up the current 10-day window into smaller time periods, as well as probing different windows, such as P14–21, or even later. The experimental model system we present in this study is uniquely suited to address these questions.

We initially "screened" Emx1-, Pvalb-, DAT-, and Dlx6a-LMO3 mice for behavioral effects of developmental hyperexcitation. We then focused on the Emx1-LMO3 mice as the group presenting with the most significant behavioral changes within the chosen test battery. For this study the other groups served as controls to rule out non-specific effects of developmental hyperexcitation. There are many more genetically defined populations that can be tested utilizing available Cre driver lines and probing the effects on a larger variety of behaviors by exploiting more extensive behavioral tests.

From our behavioral testing we had strong evidence of social deficits, and given the mPFC's known role in social behavior, we chose this area as the first region to probe in more detail in *in vivo* and *ex vivo* electrophysiological recordings. The changes observed within the mPFC are not expected to happen in mPFC alone, but rather we anticipate that they will generalize throughout the cortex, which, again, will be interesting to examine in future studies.

We are aware of the limitations of our current cortico-striatal studies. We observed robust changes in striatal activity patterns triggered on the fine-timing of neocortical spikes, a measure commonly interpreted as reflecting direct neocortical input. However, we do not know whether the reduced coupling in the developmentally hyperexcited group is due to reduced excitability of PNs, a decrease in cortico-striatal synaptic efficacy, or both. Given the reduced excitability of PNs we observed in mPFC slices, hypoexcitability of CTZ-treated PNs should contribute to the lower coupling. Definitive answers regarding the effect on synaptic efficacy in striatum can only be obtained by measuring connectivity in slices. Furthermore, spikes might be originating from neurons other than corticostriatal neurons, and the relative proportion of spikes arising from corticostriatal neurons versus other neuron types might differ in the control versus experimental groups. In this scenario, it is possible that measured spike-LFP coupling could go down even though corticostriatal coupling is actually unchanged or even increased. Yet, even if some component of the neocortically triggered signals are transmitted through a third locus (e.g., a thalamic relay), the ultimate logic of using spike-triggered analyses and downstream impact is to measure a change in effective communication, which our data do clearly suggest.

Resource availability

Lead contact

Additional resources related to this study are available upon request from the Lead Contact (Ute Hochgeschwender, hochg1u@cmich.edu).

Materials availability

Plasmids used in this study and their sequences are available at Addgene (LMO3, #114099).

Mouse lines generated in this study are available from The Jackson Laboratory (B6N.129-Gt(ROSA)26Sortm4.1(CAG-sbGLuc/COP3/EYFP)Ute, Stock No: 034853).

Data and code availability

No new code was generated in this study.

The raw datasets supporting the current study are available from the Lead Contact on request.

METHODS

All methods can be found in the accompanying Transparent Methods supplemental file.

SUPPLEMENTAL INFORMATION

Supplemental information can be found online at https://doi.org/10.1016/j.isci.2021.102157.

ACKNOWLEDGMENTS

We thank the members of the Bioluminescence Hub (http://www.bioluminescencehub.org/) for helpful discussions. This study was supported by grants from the US National Institutes of Health to U.H. (R21MH101525) and C.I.M. (U01NS099709); the National Science Foundation to U.H. and C.I.M. (NSF NeuroNex 1707352); the W.M. Keck Foundation to U.H. and C.I.M.; the Swedish Research Council to A.B. (2016-06760); and the CMU Office of Research and Graduate Studies to W.E.M. (Graduate Student Research & Creative Endeavors Grant).

AUTHOR CONTRIBUTIONS

Conceptualization, W.E.M., C.I.M., and U.H.; Methodology, W.E.M. and U.H.; Software, W.E.M.; Validation, W.E.M., A.B., C.I.M., and U.H.; Formal Analysis, W.E.M. and A.B.; Investigation, W.E.M., A.B., E.L.C., M.P., A.P., and M.L.W.; Resources, U.H.; Data Curation, W.E.M., and A.B.; Writing—Original Draft, W.E.M., C.I.M., and U.H.; Writing—Review & Editing, W.E.M., A.B., C.I.M., and U.H.; Visualization, W.E.M., A.B., and U.H.; Supervision, U.H. and C.I.M.; Project Administration, U.H.; Funding Acquisition, U.H. and C.I.M.

DECLARATION OF INTERESTS

The authors declare no competing interests.

Received: March 3, 2020
Revised: October 3, 2020
Accepted: February 3, 2021
Published: March 19, 2021

REFERENCES

Amaral, D.G. (2017). Examining the Causes of Autism. Cerebrum *2017*, cer-01-17.

Andreae, L.C., and Burrone, J. (2014). The role of neuronal activity and transmitter release on synapse formation. Curr. Opin. Neurobiol. *27*, 47–52.

Antoine, M.W., Langberg, T., Schnepel, P., and Feldman, D.E. (2019). Increased excitation-inhibition ratio stabilizes synapse and circuit excitability in four autism mouse models. Neuron *101*, 648–661.e4.

Atallah, B.V., and Scanziani, M. (2009). Instantaneous modulation of gamma oscillation frequency by balancing excitation with inhibition. Neuron *62*, 566–577.

Backman, C.M., Malik, N., Zhang, Y., Shan, L., Grinberg, A., Hoffer, B.J., Westphal, H., and Tomac, A.C. (2006). Characterization of a mouse strain expressing Cre recombinase from the 3' untranslated region of the dopamine transporter locus. Genesis *44*, 383–390.

Berglund, K., Birkner, E., Augustine, G.J., and Hochgeschwender, U. (2013). Light-emitting channelrhodopsins for combined optogenetic and chemical-genetic control of neurons. PLoS One *8*, e59759.

Berglund, K., Clissold, K., Li, H.E., Wen, L., Park, S.Y., Gleixner, J., Klein, M.E., Lu, D., Barter, J.W., Rossi, M.A., et al. (2016). Luminopsins integrate opto- and chemogenetics by using physical and biological light sources for opsin activation. Proc. Natl. Acad. Sci. U S A *113*, E358–E367.

Brunel, N., and Wang, X.J. (2003). What determines the frequency of fast network oscillations with irregular neural discharges? I. Synaptic dynamics and excitation-inhibition balance. J. Neurophysiol. *90*, 415–430.

Carlén, M., Meletis, K., Siegle, J.H., Cardin, J.A., Futai, K., Vierling-Claassen, D., Rühlmann, C., Jones, S.R., Deisseroth, K., Sheng, M., et al. (2012). A critical role for NMDA receptors in parvalbumin interneurons for gamma rhythm induction and behavior. Mol. Psychiatry *17*, 537–548.

Depino, A.M., Tsetsenis, T., and Gross, C. (2008). GABA homeostasis contributes to the developmental programming of anxiety-related behavior. Brain Res. *1210*, 189–199.

Golshani, P., Gonçalves, J.T., Khoshkhoo, S., Mostany, R., Smirnakis, S., and Portera-Cailliau, C. (2009). Internally mediated developmental desynchronization of neocortical network activity. J. Neurosci. *29*, 10890–10899.

Gomez-Ramirez, M., More, A.I., Friedman, N.G., Hochgeschwender, U., and Moore, C.I. (2020). The BioLuminescent-OptoGenetic in vivo response to coelenterazine is proportional,

sensitive, and specific in neocortex. J. Neurosci. Res. *98*, 471–480.

Gorski, J.A., Talley, T., Qiu, M., Puelles, L., Rubenstein, J.L.R., and Jones, K.R. (2002). Cortical excitatory neurons and glia, but not GABAergic neurons, are produced in the Emx1-expressing lineage. J. Neurosci. *22*, 6309–6314.

Grandjean, P., and Landrigan, P.J. (2006). Developmental neurotoxicity of industrial chemicals. Lancet (London, England) *368*, 2167–2178.

Hippenmeyer, S., Vrieseling, E., Sigrist, M., Portmann, T., Laengle, C., Ladle, D.R., and Arber, S. (2005). A developmental switch in the response of DRG neurons to ETS transcription factor signaling. PLoS Biol. *3*, e159.

Jones, K.L., and Van de Water, J. (2019). Maternal autoantibody related autism: mechanisms and pathways. Mol. Psychiatry *24*, 252–265.

Katz, L.C., and Shatz, C.J. (1996). Synaptic activity and the construction of cortical circuits. Science *274*, 1133–1138.

Kramer, M.A. (2013). An introduction to field analysis techniques: the power spectrum and coherence. In The Science of Large Data Sets: Spikes, Fields, and Voxels (Society for Neuroscience)), pp. 18–25.

Landrigan, P.J. (2010). What causes autism? Exploring the environmental contribution. Curr. Opin. Pediatr. *22*, 219–225.

Martella, G., Meringolo, M., Trobiani, L., De Jaco, A., Pisani, A., and Bonsi, P. (2018). The neurobiological bases of autism spectrum disorders: the R451C-neuroligin 3 mutation hampers the expression of long-term synaptic depression in the dorsal striatum. Eur. J. Neurosci. *47*, 701–708.

Mawson, A.R., and Croft, A.M. (2019). Rubella virus infection, the congenital rubella syndrome, and the link to autism. Int. J. Environ. Res. Public Health *16*, 3543.

Monory, K., Massa, F., Egertova, M., Eder, M., Blaudzun, H., Westenbroek, R., Kelsch, W., Jacob, W., Marsch, R., Ekker, M., et al. (2006). The endocannabinoid system controls key epileptogenic circuits in the hippocampus. Neuron *51*, 455–466.

Moore, C.I., and Berglund, K. (2020). BL-OG: BioLuminescent-OptoGenetics. J. Neurosci. Res. *98*, 469–470.

Nagarajan, N., Jones, B.W., West, P.J., Marc, R.E., and Capecchi, M.R. (2018). Corticostriatal circuit defects in Hoxb8 mutant mice. Mol. Psychiatry *23*, 1868–1877.

Nelson, S.B., and Valakh, V. (2015). Excitatory/inhibitory balance and circuit homeostasis in autism spectrum disorders. Neuron *87*, 684–698.

Park, S.Y., Song, S.H., Palmateer, B., Pal, A., Petersen, E.D., Shall, G.P., Welchko, R.M., Ibata, K., Miyawaki, A., Augustine, G.J., et al. (2020). Novel luciferase–opsin combinations for improved luminopsins. J. Neurosci. Res. *98*, 410–421.

Peca, J., Feliciano, C., Ting, J.T., Wang, W., Wells, M.F., Venkatraman, T.N., Lascola, C.D., Fu, Z., and Feng, G. (2011). Shank3 mutant mice display autistic-like behaviours and striatal dysfunction. Nature *472*, 437–442.

Peixoto, R.T., Wang, W., Croney, D.M., Kozorovitskiy, Y., and Sabatini, B.L. (2016). Early hyperactivity and precocious maturation of corticostriatal circuits in Shank3B(-/-) mice. Nat. Neurosci. *19*, 716–724.

Peixoto, R.T., Chantranupong, L., Hakim, R., Levasseur, J., Wang, W., Merchant, T., Gorman, K., Budnik, B., and Sabatini, B.L. (2019). Abnormal striatal development underlies the early onset of behavioral deficits in Shank3B(-/-) mice. Cell Rep. *29*, 2016–2027.e4.

Penn, A.A., and Shatz, C.J. (1999). Brain waves and brain wiring: the role of endogenous and sensory-driven neural activity in development. Pediatr. Res. *45*, 447–458.

Roberts, J.R., Dawley, E.H., and Reigart, J.R. (2019). Children's low-level pesticide exposure and associations with autism and ADHD: a review. Pediatr. Res. *85*, 234–241.

Romand, S., Wang, Y., Toledo-Rodriguez, M., and Markram, H. (2011). Morphological development of thick-tufted layer v pyramidal cells in the rat somatosensory cortex. Front. Neuroanat. *5*, 5.

Rothwell, P.E., Fuccillo, M.V., Maxeiner, S., Hayton, S.J., Gokce, O., Lim, B.K., Fowler, S.C., Malenka, R.C., and Sudhof, T.C. (2014). Autism-associated neuroligin-3 mutations commonly impair striatal circuits to boost repetitive behaviors. Cell *158*, 198–212.

Rubenstein, J.L.R., and Merzenich, M.M. (2003). Model of autism: increased ratio of excitation/inhibition in key neural systems. Genes, Brain Behav. *2*, 255–267.

Sasaki, T., Aoi, H., Oga, T., Fujita, I., and Ichinohe, N. (2015). Postnatal development of dendritic structure of layer III pyramidal neurons in the medial prefrontal cortex of marmoset. Brain Struct. Funct. *220*, 3245–3258.

Selimbeyoglu, A., Kim, C.K., Inoue, M., Lee, S.Y., Hong, A.S.O., Kauvar, I., Ramakrishnan, C., Fenno, L.E., Davidson, T.J., Wright, M., et al. (2017). Modulation of prefrontal cortex excitation/inhibition balance rescues social behavior in CNTNAP2-deficient mice. Sci. Transl. Med. *9*, eaah6733.

Shofty, B., Bergmann, E., Zur, G., Asleh, J., Bosak, N., Kavushansky, A., Castellanos, F.X., Ben-Sira, L., Packer, R.J., Vezina, G.L., et al. (2019). Autism-associated Nf1 deficiency disrupts corticocortical and corticostriatal functional connectivity in human and mouse. Neurobiol. Dis. *130*, 104479.

Silverman, J.L., Yang, M., Lord, C., and Crawley, J.N. (2010). Behavioural phenotyping assays for mouse models of autism. Nat. Rev. Neurosci. *11*, 490–502.

Sohal, V.S., and Rubenstein, J.L.R. (2019). Excitation-inhibition balance as a framework for investigating mechanisms in neuropsychiatric disorders. Mol. Psychiatry *24*, 1248–1257.

Song, D., Yang, Q., Lang, Y., Wen, Z., Xie, Z., Zheng, D., Yan, T., Deng, Y., Nakanishi, H., Quan, Z., et al. (2018). Manipulation of hippocampal CA3 firing via luminopsins modulates spatial and episodic short-term memory, especially working memory, but not long-term memory. Neurobiol. Learn. Mem. *155*, 435–445.

Syed, E.C.J., Sharott, A., Moll, C.K.E., Engel, A.K., and Kral, A. (2011). Effect of sensory stimulation in rat barrel cortex, dorsolateral striatum and on corticostriatal functional connectivity. Eur. J. Neurosci. *33*, 461–470.

Tartaglione, A.M., Schiavi, S., Calamandrei, G., and Trezza, V. (2019). Prenatal valproate in rodents as a tool to understand the neural underpinnings of social dysfunctions in autism spectrum disorder. Neuropharmacology *159*, 107477.

Tatavarty, V., Torrado Pacheco, A., Groves Kuhnle, C., Lin, H., Koundinya, P., Miska, N.J., Hengen, K.B., Wagner, F.F., Van Hooser, S.D., and Turrigiano, G.G. (2020). Autism-associated Shank3 is essential for homeostatic compensation in rodent V1. Neuron *106*, 769–777.e4.

Tung, J.K., Gutekunst, C.-A., and Gross, R.E. (2015). Inhibitory luminopsins: genetically-encoded bioluminescent opsins for versatile, scalable, and hardware-independent optogenetic inhibition. Sci. Rep. *5*, 14366.

Wang, X., Bey, A.L., Katz, B.M., Badea, A., Kim, N., David, L.K., Duffney, L.J., Kumar, S., Mague, S.D., Hulbert, S.W., et al. (2016). Altered mGluR5-Homer scaffolds and corticostriatal connectivity in a Shank3 complete knockout model of autism. Nat. Commun. *7*, 11459.

Yizhar, O., Fenno, L.E., Prigge, M., Schneider, F., Davidson, T.J., O'Shea, D.J., Sohal, V.S., Goshen, I., Finkelstein, J., Paz, J.T., et al. (2011). Neocortical excitation/inhibition balance in information processing and social dysfunction. Nature *477*, 171–178.

Yu, S.P., Tung, J.K., Wei, Z.Z., Chen, D., Berglund, K., Zhong, W., Zhang, J.Y., Gu, X., Song, M., Gross, R.E., et al. (2019). Optochemogenetic stimulation of transplanted iPS-NPCs enhances neuronal repair and functional recovery after ischemic stroke. J. Neurosci. *39*, 6571–6594.

Zenchak, J.R., Palmateer, B., Dorka, N., Brown, T.M., Wagner, L.M., Medendorp, W.E., Petersen, E.D., Prakash, M., and Hochgeschwender, U. (2020). Bioluminescence-driven optogenetic activation of transplanted neural precursor cells improves motor deficits in a Parkinson's disease mouse model. J. Neurosci. Res. *98*, 458–468.

iScience, Volume *24*

Supplemental information

Selective postnatal excitation of neocortical pyramidal neurons results in distinctive behavioral and circuit deficits in adulthood

William E. Medendorp, Andreas Bjorefeldt, Emmanuel L. Crespo, Mansi Prakash, Akash Pal, Madison L. Waddell, Christopher I. Moore, and Ute Hochgeschwender

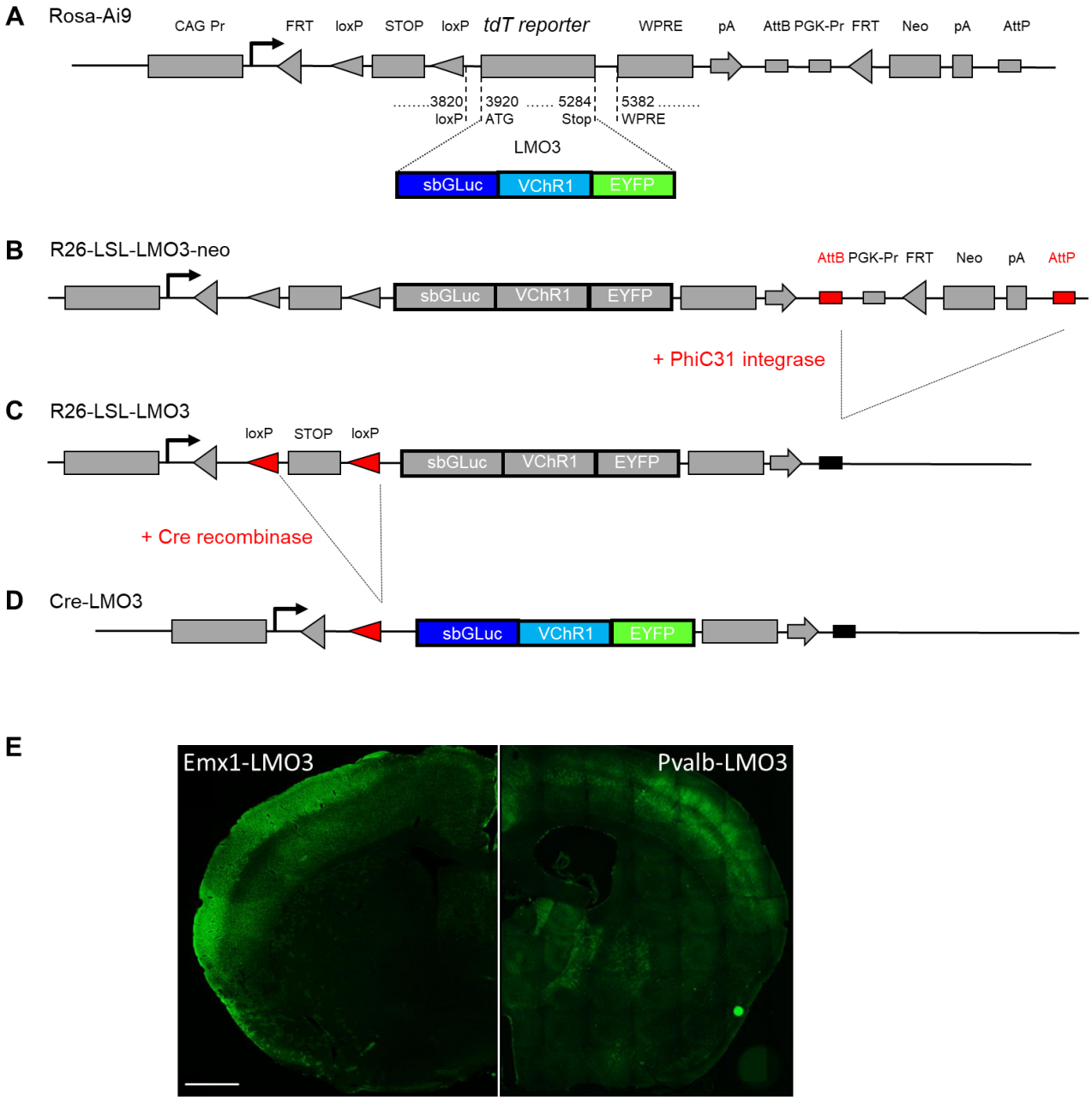

Figure S1. Conditional (lox-stop-lox) LMO3 mice, Related to Figure 1.
(A) Schematic of RosaAi9 targeting vector. The tdTomato reporter was replaced by the coding region for LMO3.
(B) Schematic of R26-LSL-LMO3-neo construct used for generating LSL-LMO3-neo embryonic stem cells and germline transmitting LSL-LMO3-neo mice.
(C) Schematic showing the modified Rosa26 locus after crossing LSL-LMO3-neo mice to PhiC31 integrase expressing mice, resulting in removal of the neo reporter in R26-LSL-LMO3 mice. These mice were crossed with the various Cre driver lines.
(D) Schematic of Rosa26 locus in cells co-expressing Cre recombinase, resulting in removal of the Stop sequence and expression of LMO3 in Cre-LMO3 mice.
(E) Fluorescence images of brain cross sections of Emx1-LMO3 (left) and Pvalb-LMO3 (right) mice. Scale bar: 1000 µm.

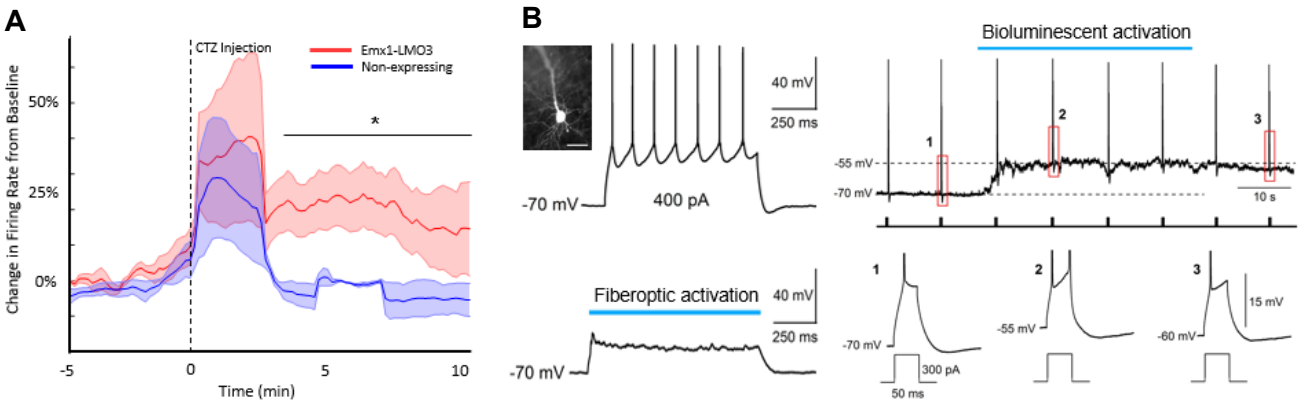

Figure S2. Bioluminescence emission causes changes in neural activity in postnatal pups *in vivo* and *ex vivo*, Related to Figure 1.
(A) Firing Rate Changes after CTZ application in P12-P14 pups. Laminar probes were inserted in the prefrontal cortex of pups aged P12 to P14 and expressing LMO3 in pyramidal neurons (Emx1-LMO3) or not. Intraperitoneal (ip) injection of CTZ during recording led to an initial non-specific increase in firing rate, after which activity in non-expressing mice went back to baseline (blue line, n=3), while Emx1-LMO3 mice showed a significant increase in firing rate (red line, n=3; $t(171) = 5.35$, $p = 2.8 \times 10^{-7}$). Shaded area represents mean ±SEM.
(B) Effect of CTZ on a prefrontal cortex layer 5 pyramidal cell expressing LMO3 at postnatal day 7. Pyramidal cell identity was confirmed through suprathreshold square current injection (800 ms, 400 pA) together with biocytin staining (left, upper panel; scale bar: 50 µm). LMO3-expression was confirmed through 480 nm light illumination delivered through the objective (30 mW/cm^2, 1 sec; left, lower panel). In these functionally immature cells action potential output required large amplitude current injections and exposure to 480 nm light evoked only subthreshold depolarization. The ability to drive excitation of young pyramidal neurons with BL-OG was tested during continuous membrane potential recording (-70 mV; maintained by continuously injecting negative DC current, <100 pA, in current clamp recording) while delivering periodic square current injections to evoke firing (0.1 Hz, 300 pA, 50 ms; right). Brief bath application of CTZ (300 µM) depolarized the membrane potential and increased the firing response to current stimulation. $*p < .05$.

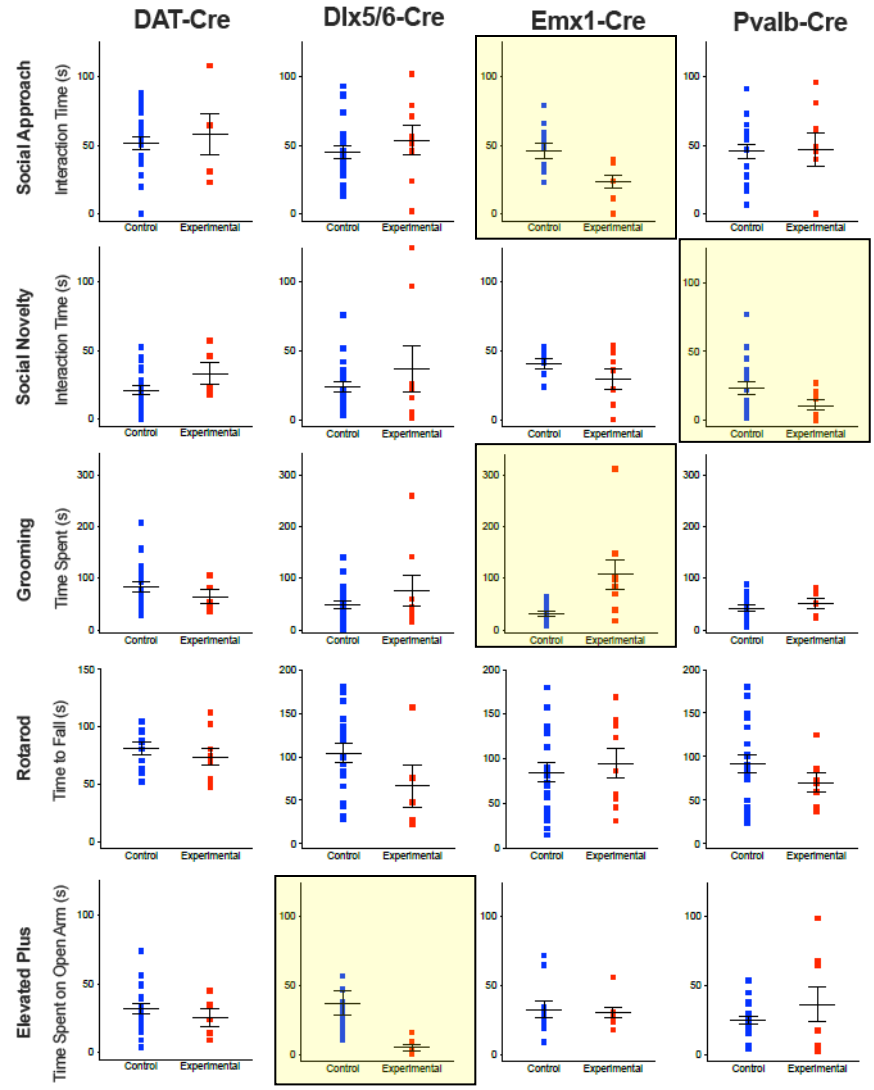
DAT-Cre
Dlx5/6-Cre
Emx1-Cre
Pvalb-Cre
Social Approach
Interaction Time (s)
Social Novelty
Interaction Time (s)
Grooming
Time Spent (s)
Rotarod
Time to Fall (s)
Elevated Plus
Time Spent on Open Arm (s)
Control
Experimental

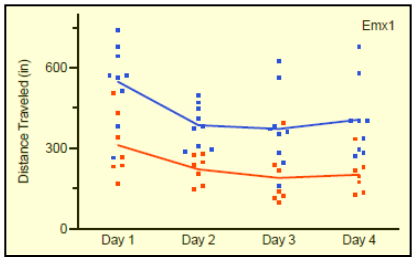
Emx1
Distance Traveled (in)
Day 1
Day 2
Day 3
Day 4

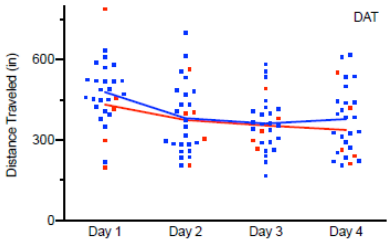
DAT
Distance Traveled (in)
Day 1
Day 2
Day 3
Day 4

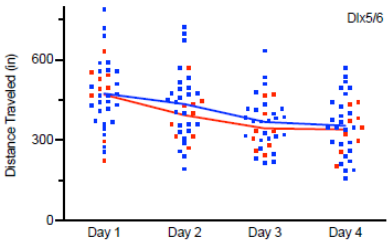
Dlx5/6
Distance Traveled (in)
Day 1
Day 2
Day 3
Day 4

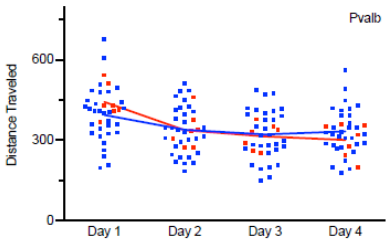
Pvalb
Distance Traveled
Day 1
Day 2
Day 3
Day 4

Figure S3. Behavioral tests, Related to Figure 1.
Results of behavioral tests showing measurements for control (non-expressing; blue color) and experimental (LMO3-expressing; red color) animals treated with CTZ during postnatal development (P4-14). These data are presented in Figure 1D as Cre (DAT, Dlx5/6, Emx1, Pvalb)-LMO3 mice normalized to their non-LMO3 expressing controls. Bars show mean ±SEM. Tests that showed significant differences are highlighted. For detailed statistics see Table S1.

Social Approach and Social Novelty: Developmentally hyperexcited Emx1-LMO3 mice show significantly reduced time interacting with the stationary mouse during the social approach test by nearly 50% compared to non-expressing littermates (students t-test: $t(18) = 3.07$, $p = 0.0067$). While Emx1-LMO3 mice display over 40% reduced time spent interacting with the novel mouse in the social novelty test compared to non-expressing littermates, these differences do not reach statistical significance (students t-test: $t(18) = 1.97$, $p = 0.0650$). In the social novelty test, Pvalb-LMO3 mice demonstrate over 50% reduced time spent interacting with the novel mouse compared to non-expressing littermates (students t-test: $t(21) = 2.19$, $p = 0.0398$, N = 8-15 per group).

Grooming: Emx1-LMO3 mice were the only group to exhibit evidence of repetitive behaviors. Emx1-LMO3 mice show significantly increased time spent grooming by 250% compared to non-expressing littermates (student's t-test: $t(18) = -2.92$, $p = 0.0091$).

Open Field: Emx1-LMO3 mice again were the only cohort to demonstrate altered exploration in open field. These mice show significantly reduced movements over time in open field (Two-way repeated measures ANOVA - Main effect between groups: $F(1,14) = 11.56$, $p = 0.0043$). All mice (expressing and non-expressing) show significant decline in movements over time, and Emx1-LMO3 show similar declines compared to non-expressing littermates (Main effect for Time: $F(11,154) = 31.30$, $p < 0.0001$; Interaction effect of Time x Group: $F(11,154) = 1.71$, $p = 0.0764$). When tested over 4 consecutive days, these results are maintained (Main effect between groups: $F(1,14) = 22.58$, $p = 0.0003$; Main effect for Time: $F(3,42) = 7.77$, $p = 0.0003$).

Table S1. Statistics, Related to Figures 1 – 3.

Figure	Group	Test	Finding	Significance
1D	Emx1-LMO3	Emx1-LMO3 vs non-expressing in social approach	reduced interaction times	students t-test: t(18) = 3.07, p = 0.0067; Two-way ANOVA: interaction effect between genotype and chamber: F(2,54) = 7.26, p = 0.0016
		Emx1-LMO3 vs non-expressing in social novelty	no significant differences versus littermate controls	students t-test: t(18) = 1.97, p = 0.0650
		Emx1-LMO3 vs non-expressing in grooming behavior	increased time spent grooming	student's t-test: t(18) = -2.92, p = 0.0091
		Emx1-LMO3 vs non-expressing in open field	reduced movements over time	Two-way repeated measures ANOVA - Main effect between groups: F(1,14) = 11.56, p = 0.0043
	Pvalb-LMO3	Pvalb-LMO3 vs non-expressing in social novelty	Reduced interaction times	Student's t-test: t(21) = 2.19, p = 0.0398
	Dlx6a-LMO3	Dlx6a-LMO3 vs non-expressing in elevated plus maze	reduced time on the open arms	log-transformed data, student's t-test: t(23) = 2.52, p = 0.0096
2B,C	Emx1-LMO3	event-related local field potentials (erLFP)	CTZ_{P4-14} mice vs VEH_{P4-14} mice: reduced amplitude during baseline	ANOVA: F(3,11752) = 51.28, p < 0.0001; Bonferroni post-hoc: p < .001
2D			CTZ_{P4-14} mice, no change in amplitude of erLFPs during light stimulus vs baseline	Bonferroni post-hoc: p = 0.913
			VEH_{P4-14} mice, increased amplitude of erLFPs during light stimulus vs baseline	Bonferroni post-hoc: p < 0.001
2E			Change in frequency of erLFPs during light stimulus vs baseline between CTZ_{P4-14} mice and VEH_{P4-14} mice	Mann-Whitney: z -1.964, p = 0.0496
			VEH_{P4-14} mice, increased frequency of erLFPs during light stimulus vs baseline	Mann-Whitney: z -1.964, p = 0.0496
2F		Power spectra	CTZ_{P4-14} vs VEH_{P4-14} mice, reduced power in the striatum	Theta: F(3,108) = 3.19, p = 0.0265; Alpha: F(3,108) = 3.48, p = 0.0184; Beta: F(3,108) = 3.40, p = 0.0204
2G - I			CTZ_{P4-14} mice, no change light stimulus vs baseline	Bonferroni post-hoc: p = 1.0
			VEH_{P4-14} mice, elevated power light stimulus vs baseline	Bonferroni post-hoc, Theta: p = 0.050; Alpha: p = 0.036; Beta: p = 0.042
2J		coherence between cortex and striatum	CTZ_{P4-14} vs VEH_{P4-14} mice, reduced coherence before and after light stimulus	Interaction of Time x Group: F(20,1128) = 1.87, p = 0.0117
3D	Emx1-LMO3	Cortical pyramidal neuron firing rate	CTZ_{P4-14} vs VEH_{P4-14} mice, larger increase in firing rate in response to light	Two-way Repeated Measures ANOVA, Main effect between groups: F(1,6) = 6.86, p = 0.0396;
			no differential effects between trials	(Main effect for trial: F(6,36) = 1.38, p = 0.2494)
			No differences in maximum firing rate between groups	Main effect between groups: F(1,6) = 1.30, p = 0.2977;
3F		pyramidal neuron firing rate	CTZ_{P4-14} vs VEH_{P4-14} mice, reduced firing rate at baseline	Students T-test: t(7) = -6.082, p = 0.0005;
			CTZ_{P4-14} vs VEH_{P4-14} mice, increased firing rate after light stimulus	t(7) = 2.541, p = 0.0386
		interneuron firing rate	CTZ_{P4-14} vs VEH_{P4-14} mice, reduced firing rate at baseline	Students T-test: t(7) = 2.526, p = 0.0395

			CTZ_{P4-14} vs VEH_{P4-14} mice, reduced firing rate after light stimulus	Students T-test: t(7) = -2.41, p = 0.0468
3G		Power spectra over time	CTZ_{P4-14} vs VEH_{P4-14} mice, increased Beta and Gamma	Beta range - Student's T-test: t(6) = 2.517, p = 0.0455; Gamma range - Student's T-test: (t(6) = 2.732, p = 0.0341
3H,I			CTZ_{P4-14} vs VEH_{P4-14} mice, reduced power in response to light stimulation in lower frequency	Two-way repeated measures – Interaction of time x group: Theta – F(20,1128) = 3.21, p < 0.0001; Alpha – F(20,1128) = 3.49, p < 0.0001; differences occurred within the first few seconds of light stimulation (Bonferroni post-hoc: Theta – p = 0.0203; Alpha – p = 0.0302)
3J			CTZ_{P4-14} vs VEH_{P4-14} mice, no difference in response to light stimulation in Beta frequency	F(20,1128) = 0.78, p = 0.7392;
3K			CTZ_{P4-14} vs VEH_{P4-14} mice, higher power in response to light stimulation in Gamma frequency	Two-way repeated measures – Interaction of time x group: F(20,1128) = 5.40, p < 0.0001;
4E	Emx1-LMO3	intrinsic firing properties	CTZ_{P4-14} vs VEH_{P4-14} mice, increased firing threshold	Students T-test: t(29) = -6.297, p < 0.0001
			CTZ_{P4-14} vs VEH_{P4-14} mice, increased rheobase current	Students T-test: t(25) = -3.494, p = 0.0017
			CTZ_{P4-14} vs VEH_{P4-14} mice, lower maximum firing frequency	Students T-test: t(25) = 5.386, p < 0.0001
			CTZ_{P4-14} vs VEH_{P4-14} mice, no effect on input resistance	Students T-test: t(25) = -0.461, p < 0.65
4G		mEPSCs	CTZ_{P4-14} vs VEH_{P4-14} mice, no change in frequency	Students T-test: t(29) = -1.167, p = 0.253
			CTZ_{P4-14} vs VEH_{P4-14} mice, no change in amplitude	Students T-test: t(29) = -0.841, p = 0.407
4I		mIPSCs	CTZ_{P4-14} vs VEH_{P4-14} mice, reduced frequency	Students T-test: t(29) = 2.414, p = 0.022
			CTZ_{P4-14} vs VEH_{P4-14} mice, reduced amplitude	Students T-test: t(29) = 2.219, p = 0.034
4J		E/I ratio	CTZ_{P4-14} mice, mPSC frequency – increased ratio	Students T-test: t(29) = -2.497, p = 0.018
			CTZ_{P4-14} mice, mPSC amplitude – increased ratio	Students T-test: t(29) = -3.457, p = 0.002
			CTZ_{P4-14} mice, synaptic drive – increased ratio	Students T-test: t(29) = -2.875, p = 0.007

TRANSPARENT METHODS

Animals

All experiments involving animals were carried out following the guidelines and protocols approved by the Institutional Animal Care and Use Committee at Central Michigan University and were in compliance with the US National Research Council's Guide for the Care and Use of Laboratory Animals, the US Public Health Service's Policy on Humane Care and Use of Laboratory Animals, and Guide for the Care and Use of Laboratory Animals.

Mice were group-housed in ventilated cages under 12-hour reverse light cycle, provided with tap water and standard chow and allowed to feed *ad libitum*.

Experimental animals were generated by crossing LSL-LMO3 mice (see below) with the following Cre driver lines: Emx1-Cre, JAX# 005628; Pvalb-Cre, JAX# 017320; Dlx5/6-Cre, JAX# 008199; DAT-Cre, JAX# 006660.

Generation of LSL-LMO3 mice

A ROSA26 targeting construct placing LMO3 (sbGLuc-VChR1-EYFP; Berglund *et al.*, 2016) under conditional (lox-stop-lox, LSL) control of the strong ubiquitous CAG promoter was generated by replacing the tdTomato gene in the Allen Brain Institute's Ai9 targeting vector (CAG-floxed tdTomato; Addgene plasmid 22799; contributed by Hongkui Zeng; Madisen et al. 2010). Embryonic stem cells were homologously targeted via electroporation of (129X1/SvJ x 129S1/Sv)F1-*Kitl*$^{+}$-derived R1 embryonic stem (ES) cells (Nagy et al., 1993), injected into blastocysts, and male chimeras were crossed with C57BL/6 females. Heterozygous LSL-LMO3 mice were further crossed to C57BL/6. The PGK-neo marker is flanked by a pair of PhiC31 recognition sites (*attB*/*attP*) and was deleted from the LSL-LMO3 line by crossing with PhiC31 deleter mice (Stock #007743, Jackson Laboratory; kindly provided by Dr. Hongkui Zeng, Allen Brain Institute). Routine genotyping for detecting the presence of the conditional alleles was done using forward primer 5'- ATGTCTGGATCCCCATCAAG, and reverse primer 5'- TCCGAAGCCAACCTTCACAGTAAC (Zhu et al., 2016). The LSL-LMO3 mouse line is available from The Jackson Laboratory (JAX#034853).

IVIS Imaging

Mouse pups aged post-natal day 4 were injected with CTZ intraperitoneally at a dose of 10µg/g. Pups were anesthetized on ice prior to being placed in the IVIS chamber. Images were taken in 5-minute bins over a 1-hour period and quantified using radiance (Perkin-Elmer, IVIS Lumina LT, Living Image Software).

Microscopy

Immunofluorescent images were captured on a Zeiss AxioCam M2 microscope using a 20x objective and digitized using the ZEN software (Carl Zeiss Inc., Thornwood, NY, USA).

Treatment of pups

The entire litter from heterozygous breeding pairs of Cre-mice and LSL-LMO3 received CTZ (water soluble native coelenterazine; Prolume Inc., cat# 3031) or vehicle (water soluble carrier without CTZ; Prolume Inc., cat# 3031C). CTZ or vehicle were injected intraperitoneally at a dose or volume equivalent of 10µg/g once per day during p4-14. Mice were then weaned, genotyped, and group-housed until used for behavioral and recording experiments.

Behavioral tests

All behavioral tests were performed with age-matched male and female littermates, starting at 2 – 3 months old and continuing over a 3-4 months period. We did not observe gender differences and thus male and female mice were pooled, generating groups of 8 – 22 animals. Mice were moved between holding room and behavioral suite, located within the same facility. Behavioral tests were carried out during the day in rooms under reverse light cycle. Testing was carried out by individuals blinded to experimental conditions. Scoring for each test was done by 2 independent individuals blinded to experimental conditions.

Three Chamber Test

Social behavior was tested using the 3-chamber test (Crawley, 2007; Yang et al., 2011). Animals were placed in a 27" x 14" chamber with 3 segments of equal size (Medendorp et al., 2018). Animals were allowed to explore the arena for 5 min to habituate to the apparatus. Mice were tested first for social approach, which has been demonstrated to relate to social deficits found in autism (Yang et al., 2011). Mice were additionally tested for social novelty immediately following the social approach test.

Social Approach: Two identical plastic cylinders were placed in either of the external chambers. These cylinders were clear, with regular holes to allow for visual and olfactory stimuli. A sex-matched, non-familiar mouse was placed in one of these cylinders. Experimental mice were placed in the middle, empty section of the 3-chamber apparatus and allowed to roam for 5 minutes. Time spent in the different chambers was measured as well as time spent interacting with the stationary mouse. Social interaction was defined by time spent within a 1-inch radius actually interacting with the stationary mouse.

Social Novelty: Following the social approach test, a novel, sex-matched, non-familiar mouse was placed in the previously empty cylinder. Experimental mice were again allowed to roam for 5 minutes. Social behavior was defined by time spent within a 1-inch radius actually interacting with the novel mouse compared to the previous mouse. The chamber was cleaned with 70% ethanol between testing mice.

Elevated Plus Maze

Mice were placed in the center of an elevated, plus-shaped apparatus (30.5" x 30.5" arms, 30.5" from the ground). Two of the external arms were covered, and 2 were open. Mice were allowed to roam the apparatus for 5 minutes. Mice were assessed for time spent on the open arms, with more time spent on the open arms indicative of less anxiety.

Open Field

Experimental mice were placed in a 17" x 9" cage and allowed to roam for 60 minutes. Movements were tracked by laser grid and analyzed using Hamilton-Kinder™ motor monitor software. Tests were repeated over 4 consecutive days using the same cage. Overall ambulation of the mice was assessed to establish normal exploratory behavior (Crawley, 1985).

Grooming Observation

Mice were observed in a 17" x 9" cage for a period of 10 minutes. Periods of grooming were noted and totaled over the 10-minute period.

Rotarod

Mice were placed on an accelerating rotarod and timed until they were unable to remain on the spinning rod. Mice were trained on the rotarod every day for 4 days prior to testing. The rotarod accelerated from 10-40 revolutions per minute (rpm) over the course of 30 seconds. At the end of the 30 seconds the

rotarod remained at 40 rpm until 180 seconds or until mice were unable to stay on the rotarod. Mice were tested for 3 trials of the rotarod and the scores averaged.

***In vivo* recording**

Mice were anesthetized with urethane at 1.5g/kg and mounted on a stereotax (Kopf Instruments). Laminar optoelectrodes were inserted in the prelimbic area of the medial prefrontal cortex (mPFC; 2mm anterior to bregma, 0.4mm lateral, and 2mm ventral). The striatal electrode (20^{o} lateral offset) was placed 0.7mm anterior to bregma, 3mm lateral, and 2.6mm ventral. Laminar probes consisted of single shank, 32-channel silicon probes with a fiber optic 50µm above the highest recording site (A1x32 Poly2-5mm-50s-177-OA32LP, Neuronexus Technologies; 0.15mm silver wire reference). Data was sampled at 30kHz and passed through a digital amplifier (Cereplex-µ, Blackrock Microsystems), and directed through HDMI to the Cereplex Direct data acquisition box (Blackrock Microsystems). Each mouse was assessed post-recording for electrode placement within both the mPFC as well as the medial dorsal striatum. Electrode placements were highly consistent between mice.

VChR1 photostimulation was carried out using a PlexBright optogenetic stimulation system (Plexon Inc.) with a blue LED module (465 nm). Mice were recorded for 20 minutes to establish a baseline. At 20 minutes, blue light was applied through the fiber optic at 300µA intensity for 10 seconds. Each light pulse was separated by 1 minute. Recordings were allowed to continue 1 hour after injection to assess response to stimulation. After recordings, brains were extracted and sectioned to confirm electrode placement.

Postnatal day 12-14 mice were anesthetized with urethane at 1g/kg and mounted on a stereotax (Kopf Instruments) via custom-made bars. Laminar electrodes (same as for adult mice) were inserted in the prelimbic area of the medial prefrontal cortex (mPFC; 0.5 mm anterior to bregma, 0.1-0.5 mm lateral to the midline; a silver wire was inserted into the cerebellum and served as ground and reference). Data was collected as above.

Coherence calculations were conducted in accordance with Kramer, 2013 in 3s bins to show the effects over time as light stimulation occurred. The Coherence calculation was started in the baseline period, where no significant differences in power were observed between CTZ- and VEH-treated mice in either the cortex or the striatum. This period also corresponds to the period where coherence is significantly different between VEH and CTZ groups. The coherence calculation encompasses the period of light stimulation, where differences in power are observed between VEH and CTZ groups; however, these periods result in no significant differences in coherence between groups.

Fast Fourier transforms were carried out using MATLAB (MATLAB FFT command). LFP waveform data were converted from time to frequency, producing power spectral density histograms. Data was pulled from a 12-second interval spanning 1second prior to light stimulus and 1 second after to encompass the entire 10 second light stimulation period. This was repeated for each light trial. Data was quantified from various frequency ranges including Delta (0-4Hz), Beta (4-8Hz), Theta (8-14Hz), and Gamma (30-100Hz).

Ex vivo recording

Acute brain slices were prepared from 4-6 week old Emx1-LMO3 mice that received daily CTZ or Vehicle injections between P4-14. A few P5-10 Emx1-LMO3 mice were included to confirm an excitatory effect of CTZ treatment during the early postnatal developmental period. Briefly, mice were anaesthetized via inhalation of isoflurane and, following decapitation, the brain was isolated and placed in ice-cold cutting solution containing (in mM): 92 NMDG, 2.5 KCl, 0.5 $CaCl_2$, 10 $MgSO_4$, 30 $NaHCO_3$, 1.25 NaH_2PO_4, 20 HEPES,

2 Thiourea, 5 Na-ascorbate, 3 Na-pyruvate and 25 D-glucose (310 mOsm/kg, pH 7.3-7.4). Coronal slices (300 µm) from prefrontal cortex were cut using a vibratome (VT1000s, Leica) and stored in a recovery solution containing (in mM): 92 NaCl, 2.5 KCl, 2 $CaCl_2$, 2 $MgSO_4$, 30 $NaHCO_3$, 1.25 NaH_2PO_4, 20 HEPES, 2 Thiourea, 5 Na-ascorbate, 3 Na-pyruvate and 25 D-glucose (310 mOsm/kg, pH 7.3-7.4). After a one hour recovery period, a slice was transferred to a recording chamber mounted on an upright microscope (BX51WI, Olympus) and perfused with aCSF containing (in mM): 121 NaCl, 2.8 KCl, 1 NaH_2PO_4, 26 $NaHCO_3$, 2 $CaCl_2$, 2 $MgCl_2$ and 15 D-glucose (310 mOsm/kg, pH 7.3-7.4) at a rate of 3 ml/min. All solutions were bubbled with a gas mixture of 95% O_2 and 5% CO_2. Whole-cell patch clamp recordings were performed using a Multiclamp 700b amplifier and Digidata 1440 digitizer together with the pClamp recording software (Molecular Devices). Borosilicate glass micropipettes were manufactured using a PC-100 puller (Narishige) and had resistances of 3–5 MΩ. Series resistance (Rs) was ≤15 MΩ in all cells after break-in and compensated by up to 70%. Rs was not allowed to fluctuate more than 25% from start to end of recording.

In current clamp recordings, pipettes were filled with intracellular solution containing (in mM): 130 K-gluconate, 10 KCl, 15 HEPES, 5 Na_2-phosphocreatine, 4 Mg-ATP, 0.3 Na-GTP and 0.5% biocytin (310 mOsm/kg, pH 7.3). Intrinsic excitability was quantified using depolarizing square current injections (800 ms, 50 pA increments) and current ramps (1 s, -200 to +500 pA) from a membrane potential of -70 mV. The aCSF was supplemented with D-AP5 (50 µM), CNQX (15 µM) and picrotoxin (100 µM) to block fast glutamatergic and GABAergic synaptic transmission. Rs was compensated using bridge balance. In voltage clamp recordings the intracellular solution contained (in mM): 130 Cs-methanesulphonate, 2 NaCl, 15 HEPES, 0.6 EGTA, 5 Qx-314, 4 Mg-ATP, 0.4 Na-GTP and 0.5% biocytin (300 mOsm/kg, pH 7.25). Miniature AMPA- and $GABA_A$-receptor mediated synaptic currents (mEPSCs and mIPSCs) were recorded at -70 and +10 mV, respectively, in presence of 100 nM tetrodotoxin. Rs was continuously monitored using a -10 mV hyperpolarizing pulse present in the recording protocol. In all recordings, Emx1-LMO3-positive prefrontal L5 pyramidal neurons were visually targeted using epifluorescence microscopy together with a CMOS camera (ORCAFusion, Hamamatsu). A current/membrane potential response to blue light was confirmed for each cell before the recording started. Excitation light (480 nm, 1 s, 30 mW/cm^2) was delivered through a 40x water immersion objective using a 130 W metal halide light source (U-HGLGPS, Olympus) and GFP filter cube (Ex/Em: 480/550 nm, U-MNIBA3, Olympus). An electronic shutter (Lambda SC, Sutter Instruments) was used to control time window of illumination.

The total number of Vehicle and CTZ treated mice used in slice recordings were 9 and 10, respectively. Data was recorded from ≤ 2 cells per brain slice, ≤ 3 slices per animal. Total number of recorded cells are indicated in Figure 4. Data was sampled at 10 kHz, filtered at 3 kHz and analyzed in Igor Pro (WaveMetrics). Action potential threshold was defined as a dV/dt of >20 mV/ms and measured on the first action potential generated from a depolarizing current ramp protocol. In frequency–current plots, firing frequency was calculated from the total number of action potentials produced during depolarizing current injections (800 ms) ranging from 0 to 500 pA. Input resistance was calculated from hyperpolarizing current injections (800 ms, -200 pA) starting from -70 mV. Miniature postsynaptic currents were analyzed blinded to experimental group in MiniAnalysis (Synaptosoft), using 5 and 10 pA event detection thresholds, respectively. mEPSCs and mIPSCs were analyzed in 2 min segments and featured a minimum of 200 events. The liquid junction potential was not corrected for.

Post hoc staining

Neurons in brain slices were pipette-filled with biocytin (0.5% w/v, Sigma-Aldrich) and fixed overnight (4°C) in PBS (0.9% NaCl) containing 4% paraformaldehyde (pH 7.3-7.4). Slices were washed 3 x 10 min in PBS (pH 7.3-7.4) and incubated in 0.25% Triton X-100 together with 5% normal goat serum (Invitrogen) for 2 h at room temperature. Following a second wash the slices were incubated in streptavidin-CY5 (1:300, Invitrogen), 0.25% Triton X-100 and 5% normal goat serum for 2 h at room temperature. After a final wash, slices were mounted on slides and cover slipped with ProLong Gold mounting medium (Thermo Fisher). Streptavidin-CY5-labelled cells were imaged on an Axio Imager M2 microscope (Zeiss) using 10x, 20x and 40x air objectives.

Quantification and Statistical Analysis

All analysis was carried out using MATLAB and SPSS software. Data are displayed as mean±standard error of the mean (SEM). Behavior tests were tested using Student's t-test between expressing and non-expressing mice. The three-chamber tests were also analyzed with two-way ANOVA. Open field was tested using two-way repeated measures ANOVAs.

Electrophysiological *in vivo* data was high pass filtered at 250Hz to extract spikes and low pass filtered at 300Hz to extract LFPs. Spike data was thresholded at -63µV and sorted for each channel based on waveform characteristics using Principal Components Analysis (PCA). Spikes were binned to calculate frequency of firing over time. Differences between groups were assessed using two-way repeated measures ANOVAs (repeat trials per mouse). For *ex vivo* electrophysiological data, statistical significance between groups was determined using Student's T-test.

Supplemental References

Crawley, J.N. (1985). Exploratory behavior models of anxiety in mice. Neurosci. Biobehav. Rev. *9*, 37–44.

Crawley, J.N. (2007). What's Wrong With My Mouse?: Behavioral Phenotyping of Transgenic and Knockout Mice (John Wiley & Sons).

Madisen, L., Zwingman, T.A., Sunkin, S.M., Oh, S.W., Zariwala, H.A., Gu, H., Ng, L.L., Palmiter, R.D., Hawrylycz, M.J., Jones, A.R., et al. (2010). A robust and high-throughput Cre reporting and characterization system for the whole mouse brain. Nat. Neurosci. *13*, 133–140.

Medendorp, W.E., Petersen, E.D., Pal, A., Wagner, L.-M., Myers, A.R., Hochgeschwender, U., and Jenrow, K.A. (2018). Altered Behavior in Mice Socially Isolated During Adolescence Corresponds With Immature Dendritic Spine Morphology and Impaired Plasticity in the Prefrontal Cortex. Front. Behav. Neurosci. *12*, 87.

Nagy, A., Rossant, J., Nagy, R., Abramow-Newerly, W., and Roder, J.C. (1993). Derivation of completely cell culture-derived mice from early-passage embryonic stem cells. Proc. Natl. Acad. Sci. U. S. A. *90*, 8424–8428.

Yang, M., Silverman, J.L., and Crawley, J.N. (2011). Automated three-chambered social approach task for mice. Curr. Protoc. Neurosci. *Chapter 8*, Unit 8.26.

Zhu, H., Aryal, D.K., Olsen, R.H.J., Urban, D.J., Swearingen, A., Forbes, S., Roth, B.L., and Hochgeschwender, U. (2016). Cre-dependent DREADD (Designer Receptors Exclusively Activated by Designer Drugs) mice. Genesis *54*, 439–446.